

Shape Curvature Histogram: A Shape Feature for Celiac Disease Diagnosis

Michael Gadermayr, Michael Liedlgruber, Andreas Uhl, and Andreas Vécsei

Department of Computer Sciences, University of Salzburg, Austria
{mgadermayr,mliedl,uhl}@cosy.sbg.ac.at

Abstract. In this work we introduce a curvature based shape feature extraction technique, which unlike others, does not necessarily depend on a closed boundary or a defined region. While the proposed feature has been developed for celiac disease diagnosis, it can potentially be utilized in other problem domains as well.

To construct the proposed descriptor, first an input color channel is subject to edge detection and gradient computations. Then, based on the gradient map and edge map, the local curvature is computed for each pixel as the angular difference between the maximum and minimum gradient angle within a certain neighborhood.

Experiments show, that the feature is competitive as far as the classification rate is concerned. Despite its discriminative power, a further positive aspect is the compactness of the feature vector.

1 Introduction

Celiac disease is a complex autoimmune disorder in genetically predisposed individuals of all age groups after introduction of gluten containing food. Commonly known as gluten intolerance, this disease has several other names in literature, including cœliac disease, c(o)eliac sprue, non-tropical sprue, endemic sprue, gluten enteropathy or gluten-sensitive enteropathy. The real prevalence of the disease has not been fully clarified yet. This is due to the fact that most patients with celiac disease suffer from no or atypical symptoms and only a minority develops the classical form of the disease. Since several years, prevalence data have been continuously adjusted upwards. Fasano et al. state that more than 2 million people in the United States, this is about one in 133, have the disease [1].

Endoscopy with biopsy is currently considered the gold standard for the diagnosis of celiac disease. Due to the technological advances in endoscopy throughout the past years, modern endoscopes also allow to capture images, which facilitates automated analysis and diagnosis. Thus, automated classification as a support tool is an emerging option for endoscopic diagnosis and treatments [2].

In the past various different approaches for an automated classification of celiac disease images have been proposed. The majority of these approaches investigated different texture features for the classification. Features utilized throughout these works include for example simple statistical features [3], statistical features on color histograms [4], statistical features extracted from Fourier

magnitudes [5]. In the studies presented in [6] and [7] an extensive comparison between various different types of features (e.g. wavelet-based, Fourier-based, Random fields, and Local Binary Pattern variants) has been conducted. In [7] two shape-based approaches have been evaluated [8, 9], which – to the best of our knowledge – are the only two shape-based approaches ever evaluated for an automated diagnosis of celiac disease. Actually, there exists different definitions of shape-based features. In this paper, shape-based features are those, which are based on a previous segmentation of sound objects in the image.

Compared to the results obtained with the texture features the shape-based feature proposed in [8] yielded rather poor results only. The main cause for this is the fact that this feature has been specifically tailored to another problem domain (i.e. colonic polyp classification). Although the second shape-based feature (from [9]) performed rather well in terms of the classification rates achieved, it must be pointed out that this approach is based on a feature selection, which is an advantage compared to the other approaches evaluated.

In this work we present a novel shape-based feature, called Shape Curvature Histogram (SCH). This feature describes the curvature of shapes found within an image in the form of a compact descriptor. In contrast to many other shape-based features the SCH feature does not require shapes with closed boundaries which could be difficult or even impossible to obtain if single objects cannot be identified. Thereby our approach is a very general one and can potentially be applied to other problem domains as well.

To compute the SCH, first a binary edge map based on the input image is generated. This is followed by computing the direction of the gradient for each edge pixel. Then for each edge pixel the maximum difference between the gradient directions within a certain neighborhood around this pixel is computed. The final descriptor is then obtained by generating a histogram over the differences for all edge pixels.

The remaining part of this paper is organized as follows: In Section 2 a brief overview of the medical background behind celiac disease is given, followed by an explanation of the details behind SCH in Section 3 and a brief coverage of the classification setup in Section 4. In Section 5 we show that the proposed method is applicable to our problem. High classification rates imply a high discriminative power even with a very compact feature representation. Section 6 concludes this paper.

2 Medical Background

The gastrointestinal manifestations in case of celiac disease invariably comprise an inflammatory reaction within the mucosa of the small intestine caused by a dysregulated immune response triggered by ingested gluten proteins of certain cereals (wheat, rye, and barley), especially against gliadine. During the course of the disease, hyperplasia of the enteric crypts occurs and the mucosa eventually loses its absorptive villi thus leading to a diminished ability to absorb nutrients. People with untreated celiac disease, even if asymptomatic, are at risk for devel-

oping various complications like osteoporosis, infertility and other autoimmune diseases including type 1 diabetes, autoimmune thyroid disease and autoimmune liver disease.

During standard upper endoscopy at least four duodenal biopsies are taken. Microscopic changes within these specimen are then histologically classified according to the modified Marsh classification, as proposed by Oberhuber et al. [10]. This classification is based on a scheme originally proposed by Marsh in 1992 [11]. The modified Marsh classification distinguishes between classes Marsh-0 to Marsh-3, with subclasses Marsh-3a, Marsh-3b, and Marsh-3c, resulting in a total number of six classes.

According to the modified Marsh classification Marsh-0 denotes a healthy mucosa (without visible changes of the villous structure) and Marsh-3c designates a complete absence of villi (villous atrophy). Table 1 briefly summarizes the characteristic changes of the mucosal tissue caused by celiac disease.

Table 1. Characteristic changes of mucosal tissue caused by celiac disease.

Marsh class	Characteristic changes
0-2	No visible changes of villi structure
3a	Mild villous atrophy
3b	Marked villous atrophy
3c	Absent villi

Figure 1 shows example images for the different Marsh classes. From these images we clearly notice the villous atrophy in classes Marsh-3a to Marsh-3c, while the villi show up very clear in case of Marsh-0.

Since there are no visual differences between Marsh-0, Marsh-1, and Marsh-2, we consider Marsh-0 and Marsh-3a to Marsh-3c only throughout this paper. Moreover, we restrict our experiments to a classification between healthy patients (i.e. Marsh-0) and those who are affected by celiac disease (i.e. Marsh-3a to Marsh-3c).

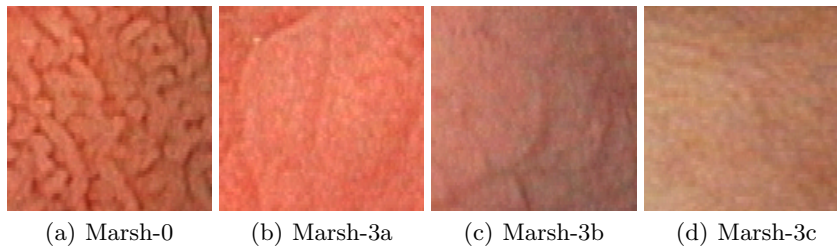


Fig. 1. Examples images for the different Marsh classes.

3 Shape Curvature Histogram (SCH)

The computation of the SCH feature can be divided into the following steps: edge map generation, orientation computation, curvature computation, and the creation of the final feature vector.

In the explanations below I denotes the image the SCH feature should be computed for. If I is a grayscale image the computation steps are carried out only once, resulting in a single histogram. For RGB images the steps are carried out for each color channel separately, resulting in one histogram for each color channel. These histograms are then concatenated in order to obtain the final feature vector.

In the following we explain the computation steps in more detail.

3.1 Edge Map Generation

To be able to compute the curvature information the first step is the generation of an edge map. For this purpose we employ the Canny edge detector [12]. The result of the edge detection is an edge map which contains all pixel for which we compute the curvature values. In other words, pixels which do not belong to an edge are masked out from the computation steps below.

Although in special cases the edge map might contain closed boundaries, generally the edge map could consist of an arbitrary number of disconnected parts of arbitrary shapes. Thus, we can not make any assumption on the existence of closed boundaries, which would be obligate for contour-based or region-based shape feature extraction techniques.

3.2 Computation of Orientation

Once the edge map is generated, we compute the gradient direction for each edge pixel. Having both partial derivatives, this direction can be calculated as ¹

$$\Theta(x, y) = \text{atan2} \left(\frac{\partial I}{\partial y}(x, y), \frac{\partial I}{\partial x}(x, y) \right), \quad (1)$$

where (x, y) denotes the position of the edge pixel for which the orientation is computed. The resulting values for $\Theta(x, y)$ always lie within the range $(-\pi, \pi]$.

The partial derivatives $\frac{\partial I}{\partial x}$ and $\frac{\partial I}{\partial y}$ are approximated by a convolution of the image with Sobel filters. Figure 2(e) shows an example orientation image, which has been computed from the example image shown in Fig. 2(a) and the edge map shown in Fig. 2(b).

¹ The function `atan2` denotes the four-quadrant implementation of the `atan`-function in MATLAB.

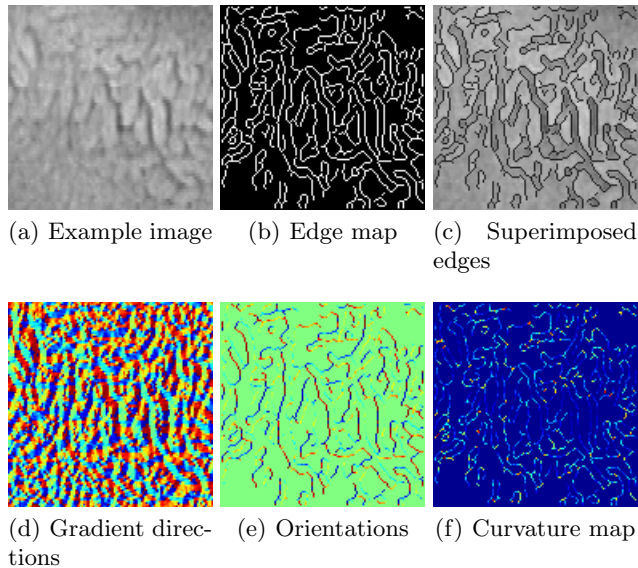


Fig. 2. Output of the different steps when extracting the SCH feature for a grayscale image. (a) the input image, (b) the corresponding edge map, (c) the edge map superimposed to the input image, (d) the gradient directions for the input image, (e) the edge pixel orientations, and (f) the final image showing the curvature values for the edge pixels (based on a 3×3 -neighborhood).

3.3 Computation of Curvature

Having the orientation for each edge pixel, we compute the curvature for an edge pixel as the difference between the maximum and minimum gradient angle over all edge pixels within a certain neighborhood. The curvature C for an edge pixel located at (x, y) can thus be formulated as:

$$C(x, y) = D(\Theta_{\min}(x, y), \Theta_{\max}(x, y)), \quad (2)$$

with

$$\Theta_{\min}(x, y) = \min_{(i,j) \in N(x,y)} \Theta(i, j) \quad (3)$$

and

$$\Theta_{\max}(x, y) = \max_{(i,j) \in N(x,y)} \Theta(i, j), \quad (4)$$

where $N(x, y)$ denotes the set of pixel positions of edge pixels within an $w \times w$ -neighborhood centered at (x, y) (w denotes the width and height of the neighborhood).

The difference between two arbitrary gradient directions might yield two different types of angles: either an angle in the range $[0, \pi]$ or the respective reflex angle in the range $(\pi, 2\pi]$. Since we are only interested in angle differences in the

range $[0, \pi]$, we quite often need to compute the smaller angle from the reflex angle. Hence, we use the following formula to compute the difference between two angles α and β :

$$D(\alpha, \beta) = \begin{cases} \Delta(\alpha, \beta), & \text{if } \Delta(\alpha, \beta) \leq \pi, \\ 2\pi - \Delta(\alpha, \beta), & \text{if } \Delta(\alpha, \beta) > \pi \end{cases}, \quad (5)$$

with

$$\Delta(\alpha, \beta) = \max(\alpha, \beta) - \min(\alpha, \beta). \quad (6)$$

A schematic illustration of the pixel-wise curvature computation is provided in Fig. 3.

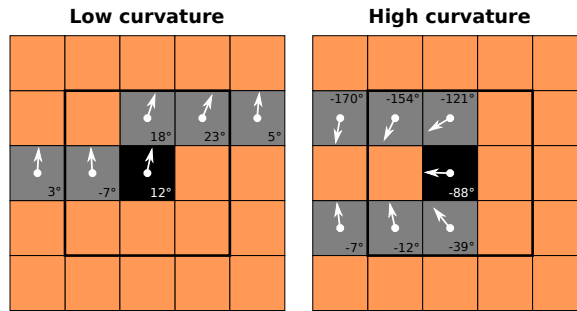


Fig. 3. Computation of the curvature for a pixel (black, filled square). The gradient directions for the edge pixels (shown in dark gray) are indicated by arrows (the according angles are given in degrees). The 3×3 -neighborhood used in this example is indicated by a black square. While the left image shows an example for a low curvature value ($C(x, y) = 30^\circ$), the right image shows a rather high curvature ($C(x, y) = 142^\circ$).

Figure 2(f) shows an example for a curvature map based on the input image shown in Fig. 2(a). In this figure, blue pixels denote a low curvature whereas red pixels denote a high curvature value.

3.4 Generation of Feature Vector

Based on the curvature values for the edge pixels a histogram based on these values is created.

For the construction of a histogram we do not consider curvature values of non-edge pixels since these contain no information anyway (due to the restriction of the curvature computation to edge pixels). Hence, the number of pixels contributing to the curvature histogram is likely to change from image to image. As a consequence we normalize each histogram by the number of edge pixels found in the respective image.

The limits of the histograms cover the complete range of possible curvature values (i.e. $[0, \pi]$). The number of bins to be used for histogram creation can be

adjusted. The higher the number of bins the more detailed the curvature values get captured by the resulting histogram. But the length of the resulting feature vectors will also be higher. In addition, in case of too many bins the bin values may get rather noisy, making the feature unstable in terms of the classification. If, in contrast, the number of bins is too low potentially discriminative information may get lost in the histogram, with the advantage of a more compact descriptor.

In our experiments we use 8 bins for our histograms, which yields high classification results although the feature vectors are pretty compact. The choice for the number of bins corresponds to a range of $\pi/8$ (i.e. 22.5°) covered by each bin.

4 Classification

To estimate the classification accuracy of our system we use leave-one-patient-out cross-validation (LOPO-CV). In this setup one image out of the database is considered as an unknown image. The remaining images are used to train the classifier (omitting those images which originate from the same patient as the image left out). The class of the unknown image is then predicted by the system. These steps (training and prediction) are repeated for each image, yielding an estimate of the overall classification accuracy.

To actually classify an unknown image (not contained in the training set) we use the k-nearest-neighbor classifier (k-NN). This rather weak classifier has been chosen to emphasize more on quantifying the discriminative power of the features proposed in this work.

To measure the distance between two histograms we employ the histogram intersection distance metric, defined as

$$d(H_i, H_j) = 1 - \sum_{k=1}^B \min(H_{i,k}, H_{j,k}), \quad (7)$$

where H_i and H_j are two normalized histograms, B denotes the number of bins used in our histograms, and $H_{i,k}$ and $H_{j,k}$ represent the value of the k -th bin of histogram H_i and H_j , respectively. We also carried out experiments using other distance metric (the Euclidean distance metric and the Bhattacharyya distance metric) but the classification results were rather similar to those obtained with the histogram intersection distance metric. Hence, since the histogram intersection can be computed more efficiently as compared to the two other alternatives, we decided to use this distance metric for our experiments.

5 Experiments

5.1 Experimental Setup

The image database used throughout our experiments is based on images taken during duodenoscopies at the St. Anna Children’s Hospital, using pediatric

gastrosopes without magnification (GIF-Q165 and GIF-N180, Olympus, Hamburg). The main indications for endoscopy were the diagnostic evaluation of dyspeptic symptoms, positive celiac serology, anemia, malabsorption syndromes, inflammatory bowel disease, and gastrointestinal bleeding. Images were recorded by using the modified immersion technique, which is based on the instillation of water into the duodenal lumen for better visibility of the villi. Using this technique, the tip of the gastroscope is inserted into the water and images of interesting areas are taken. A study [13] shows that the visualization of villi with the immersion technique has a higher positive predictive value. Previous work [6] also found that the modified immersion technique is more suitable for automated classification purposes as compared to the classical image capturing technique.

To study the prediction accuracy of different features we manually created an “idealistic” set of textured image patches with optimal quality. Thus, the captured data was inspected and filtered by several qualitative factors (sharpness, distortions, and visibility of features). In the next step, texture patches with a fixed size of 128×128 pixels were extracted (a size which turned out to be optimally suited in earlier experiments on automated celiac disease diagnosis [6]). This way we created an extended set containing more images available for classification.

In order to generate ground truth for the texture patches used in experimentation, the condition of the mucosal areas covered by the images was determined by histological examination of biopsies from the corresponding regions. Severity of villous atrophy was classified according to the modified Marsh classification.

Table 2. The detailed ground truth information for the celiac disease image database used throughout our experiments.

	$N_{\mathbf{O}}$	$N_{\mathbf{E}}$	$N_{\mathbf{P}}$
No celiac	234	306	131
Celiac	172	306	40
Total	406	612	171

Table 2 shows the detailed ground truth information used for our experiments where $N_{\mathbf{O}}$, $N_{\mathbf{E}}$, $N_{\mathbf{P}}$ denote the number of original images, the number of images in the extended image set, and the number of patients in each class, respectively.

Since the optimal choices for the k -value for the k -NN classifier are not known at beforehand, we decided to carry out an exhaustive search for the k -value which leads to the highest overall classification rates ($k \in 1, \dots, 50$). Apart from that we carry out experiments with grayscale images as well as with RGB color images. In order to compute the local curvature values (see Equ. (2)), we used a 3×3 -neighborhood. While bigger neighborhoods are theoretically possible, experiments showed that, especially in case of dense edge maps (i.e. a high number of edge pixels), bigger neighborhoods are more likely to interfere with edge pixels from different edges.

We also aim at a comparison between the proposed method and a set of four features proposed in the past. These features include texture-based features as well as shape-features:

– **Graylevel Co-occurrence Matrix features (GLCM) [14]**

The GLCM is a 2D-histogram, which describes the spatial relationship between neighboring pixels. The matrix is created based on the co-occurring values of pixels across an image (for some fixed pixel offset). In other words, for each possible combination of two pixel values the GLCM stores the number of co-occurrences within an image for a given displacement between the pixels. While the displacement is fixed for a single GLCM, it can be adjusted with respect to the pixel distance (one pixel in our experiments) and the direction.

To obtain features for the classification, we compute a GLCM for four different directions (up, down, left, and right) and compute a subset of the statistical features proposed in [14] (i.e. contrast, correlation, energy, and homogeneity) on each GLCM. The final features used are composed by concatenating the Haralick features extracted.

– **Edge Co-occurrence Matrix (ECM) [15]**

After applying eight differently orientated directional filters (rotated Sobel filters) on the source image a gradient magnitude image is constructed for each direction. Based on these the direction with the maximum response is determined for each pixel, followed by masking out pixels with a gradient magnitude below some threshold (75% below the maximum response in our experiments). Then the methodology of GLCM is used to obtain the ECM for one specific displacement (one pixel displacement in our experiments). As suggested in [15], we compute the element-wise sum of eight ECMs (one for each direction) to obtain the final ECM for one specific displacement distance.

– **Local Binary Patterns (LBP) [16]**

Local binary patterns are a powerful method to describe local texture properties within an image. In its simplest form, this method compares the grayscale value of a pixel to the values of the eight nearest neighbors. If the value of a neighbor exceeds the center pixel value the respective neighborhood position is set to one. The number resulting from the neighborhood bit sequence corresponds to the LBP number. In other words, the neighbors of each pixel are thresholded by the respective center pixel and the resulting binary sequence is used to obtain the final LBP number. Based on the LBP numbers computed for all pixels in the source image a histogram is generated, which then serves as the feature vector.

– **Shape features combination (EDGEFEATURES) [9]**

After Canny Edge detection, different features from edge-enclosed regions are computed. In the original paper [9] we used edge shape features as well as texture features. For the results in this work we slightly modified this method to restrict the features to shape features. To find the most discriminative combination of features we use a greedy forward feature subset selection.

Since our image database is quite limited in terms of the number of images available, we employ the leave-one-patient-out cross-validation (LOPO-CV). Hence, the images from one patient are removed from the image set (serving as the validation samples) while the remaining images are used to train the underlying classifier. This process is repeated for all patients in the image database.

In order to be able to assess whether two different methods produce statistically significant differences in the results obtained, we employ McNemar’s test [17]. For two methods M_1 and M_2 this test statistic keeps track of the number of images which are misclassified by method M_1 but classified correctly by method M_2 (denoted by n_{01}) and vice versa (denoted by n_{10}). The test statistic, which is approximately Chi Square distributed (with one degree of freedom), is then computed as

$$T = \frac{(|n_{01} - n_{10}| - 0.5)^2}{n_{01} + n_{10}}. \quad (8)$$

From T the p -value can be computed as

$$p = 1 - F_{\chi_1^2}(T) \quad (9)$$

where $F_{\chi_1^2}$ denotes the cumulative distribution function of the Chi Square distribution with one degree of freedom. The null-hypothesis H_0 for McNemar’s test is that the outcomes of M_1 and M_2 lead to equal error rates. Given a fixed significance level α , there is evidence that the methods M_1 and M_2 produce significantly different results if $p < \alpha$. As a consequence we can reject the null-hypothesis H_0 . Throughout this work we chose a significance level of $\alpha = 0.05$. This implies that, if M_1 and M_2 are significantly different, there is a confidence level of 95% that the differences between the outcomes of the methods are not caused by random variation.

5.2 Results

Table 3 shows the detailed results for our experiments. The column “SD” in this table indicates whether there is a statistically significant difference between the results obtained with the SCH method and the other methods according to McNemar’s test. In addition, the sign given in brackets indicates whether the results obtained are significantly lower (–) or significantly higher (+) as compared to the results of the SCH method. The last column (SCS) provides the information whether there is a statistically significant difference between the results for a specific method when comparing the grayscale and color results.

From these results we immediately notice that the SCH feature yields the highest overall classification rate (accuracy) as compared to the other features. This accounts to the results with grayscale images as well as to the color images results. We also notice that SCH in most cases delivers significantly higher results when compared to the other methods. Only in case of LBP applied to the grayscale images the difference to SCH is not significant, although also in this case SCH delivers a higher classification accuracy.

Table 3. Detailed classification rates obtained for grayscale images and color images.

Grayscale Images					
Method	Accuracy	Specificity	Sensitivity	SD	SCS
SCH	87.58	89.87	85.29		
ECM	77.45	75.16	79.74	✓ (-)	
GCM	73.69	67.97	79.41	✓ (-)	
LBP	84.97	82.35	87.58		✓ (-)
EDGEFEATURES	67.16	75.49	58.82	✓ (-)	
RGB Color Images					
Method	Accuracy	Specificity	Sensitivity	SD	SCS
SCH	85.78	89.22	82.35		
ECM	76.31	78.10	74.51	✓ (-)	
GCM	75.98	74.84	77.12	✓ (-)	
LBP	81.54	80.72	82.35	✓ (-)	✓ (+)
EDGEFEATURES	70.92	75.82	66.01	✓ (-)	

We also see that there are two methods only, which deliver a slightly higher accuracy when extracting the features from color images (i.e. GCM and EDGEFEATURES). In case of all other methods we observe a slight decrease of the accuracy in case of color images. But, except for the LBP method, the differences observed are not significantly different.

When looking at the results yielded by the EDGEFEATURES method we notice that the results are considerably lower as compared to the SCH method. This is especially interesting since the EDGEFEATURES method employs a feature selection algorithm, which – at least theoretically – should be advantageous.

6 Conclusion

We proposed a novel shape-based feature which we successfully applied to the problem of an automated celiac disease diagnosis. We showed that, although the descriptor used is very compact, we in most cases achieve significantly higher classification accuracies as compared to some well-established feature extraction methods (texture features as well as shape-based features).

We also showed that the SCH method can be easily extended to work with RGB color images. However, compared to the accuracy in case of grayscale images, the accuracy changes observed in our experiments are not statistically significant.

Since the proposed feature has not been tailored specifically to celiac disease images (i.e. it makes no assumptions about the edges and gradients used), it may be potentially applied to other problem domains as well.

References

1. Fasano, A., Berti, I., Gerarduzzi, T., Not, T., Colletti, R.B., Drago, S., Elitsur, Y., Green, P.H.R., Guandalini, S., Hill, I.D., Pietzak, M., Ventura, A., Thorpe, M.,

- Kryszak, D., Fornaroli, F., Wasserman, S.S., Murray, J.A., Horvath, K.: Prevalence of celiac disease in at-risk and not-at-risk groups in the united states: a large multicenter study. *Archives of internal medicine* **163** (February 2003) 286–92
2. Liedlgruber, M., Uhl, A.: Computer-aided decision support systems for endoscopy in the gastrointestinal tract: A review. *IEEE Reviews in Biomedical Engineering* **4** (2012) 73–88
 3. Ciaccio, E.J., Tennyson, C.A., Lewis, S.K., Krishnareddy, S., Bhagat, G., Green, P.H.: Distinguishing patients with celiac disease by quantitative analysis of video-capsule endoscopy images. *Computer Methods and Programs in Biomedicine* **100**(1) (October 2010) 39–48
 4. Vécsei, A., Fuhrmann, T., Uhl, A.: Towards automated diagnosis of celiac disease by computer-assisted classification of duodenal imagery. In: Proceedings of the 4th International Conference on Advances in Medical, Signal and Information Processing (MEDSIP '08), Santa Margherita Ligure, Italy (2008) 1–4 paper no P2.1-009.
 5. Vécsei, A., Fuhrmann, T., Liedlgruber, M., Brunauer, L., Payer, H., Uhl, A.: Automated classification of duodenal imagery in celiac disease using evolved fourier feature vectors. *Computer Methods and Programs in Biomedicine* **95** (August 2009) S68–S78
 6. Hegenbart, S., Kwitt, R., Liedlgruber, M., Uhl, A., Vécsei, A.: Impact of duodenal image capturing techniques and duodenal regions on the performance of automated diagnosis of celiac disease. In: Proceedings of the 6th International Symposium on Image and Signal Processing and Analysis (ISPA '09), Salzburg, Austria (September 2009) 718–723
 7. Gschwandtner, M., Liedlgruber, M., Uhl, A., Vécsei, A.: Experimental study on the impact of endoscope distortion correction on computer-assisted celiac disease diagnosis. In: Proceedings of the 10th International Conference on Information Technology and Applications in Biomedicine (ITAB'10), Corfu, Greece (November 2010)
 8. Häfner, M., Gangl, A., Liedlgruber, M., Uhl, A., Vécsei, A., Wrba, F.: Classification of endoscopic images using Delaunay triangulation-based edge features. In: Proceedings of the International Conference on Image Analysis and Recognition (ICIAR'10). Volume 6112 of Springer LNCS., Povo de Varzim, Portugal (June 2010) 131–140
 9. Häfner, M., Gangl, A., Liedlgruber, M., Uhl, A., Vécsei, A., Wrba, F.: Endoscopic image classification using edge-based features. In: Proceedings of the 20th International Conference on Pattern Recognition (ICPR'10), Istanbul, Turkey (August 2010) 2724–2727
 10. Oberhuber, G., Granditsch, G., Vogelsang, H.: The histopathology of coeliac disease: time for a standardized report scheme for pathologists. *European Journal of Gastroenterology and Hepatology* **11** (November 1999) 1185–1194
 11. Marsh, M.: Gluten, major histocompatibility complex, and the small intestine. a molecular and immunobiologic approach to the spectrum of gluten sensitivity ('celiac sprue'). *Gastroenterology* **102**(1) (1992) 330–354
 12. Canny, J.: A computational approach to edge detection. *IEEE Transactions on Pattern Recognition and Machine Intelligence* **8**(6) (September 1986) 679–698
 13. Gasbarrini, A., Ojetti, V., Cuoco, L., Cammarota, G., Migneco, A., Armuzzi, A., Pola, P., Gasbarrini, G.: Lack of endoscopic visualization of intestinal villi with the immersion technique in overt atrophic celiac disease. *Gastrointestinal endoscopy* **57** (March 2003) 348–351

14. Haralick, R.M., Shanmugam, K., Dinstein, I.: Textural features for image classification. *IEEE Transactions on Systems, Man, and Cybernetics* **3** (1973) 610–621
15. Rautakorpi, R., Iivarinen, J.: A novel shape feature for image classification and retrieval. In: *Proceedings of the International Conference on Image Analysis and Recognition (ICIAR'04)*. (2004) 753–760
16. Ojala, T., Pietikäinen, M., Harwood, D.: A comparative study of texture measures with classification based on feature distributions. *Pattern Recognition* **29**(1) (January 1996) 51–59
17. Everitt, B.: *The Analysis of Contingency Tables*. Chapman and Hall (1977)